ACS APPLIED MATERIALS & INTERFACES

Research Article

www.acsami.org

Plasmon Induced Nano Au Particle Decorated over S,N-Modified TiO_2 for Exceptional Photocatalytic Hydrogen Evolution under Visible Light

Soumyashree Pany,[†,‡] Brundabana Naik,[‡] Satyabadi Martha,[‡] and Kulamani Parida*[,†,‡]

[†]Academy of Scientific and Innovative Research, New Delhi-110 001, India

[‡]Colloids and Materials Chemistry Department, CSIR-Institute of Minerals and Materials Technology, Bhubaneswar-751 013, Odisha, India

ABSTRACT: Nano Au deposited mesoporous S,N-TiO_2 (SNT) nanocomposites have been fabricated through deposition precipitation technique by employing urea as the hydrolyzing agent. To investigate the structural, optical, and electronic properties, the photocatalysts are characterized through X-ray diffraction (XRD), UV−vis diffuse reflectance spectra, transmission electron microscopy (TEM), X-ray photoelectron spectroscopy (XPS), and photoelectrochemical measurements. Here in addition to the co-catalyst nature of nano Au particles, surface plasmon resonance (SPR) effect in visible region enhances the light harvestation ability as well as transfer electrons to the conduction band of SNT. Furthermore, easy channelization of photogenerated charge carriers through sulfate facilitated redox couple makes the system more potential towards H_2 evolution. TEM study exhibits well interconnective morphology in the matrix which helps easy channelization of electrons in the SNT nanocomposites. The photocatalytic activities have been evaluated for hydrogen generation under the irradiation of visible light and an enhanced activity has been observed for the Au promoted SNT due to the presence of nano Au particles, that is, 3.5 nm. The hydrogen generation activity of 3Au-SNT is nearly 9 times higher than that of neat SNT, and the energy conversion efficiency was found to be 17.6 %.

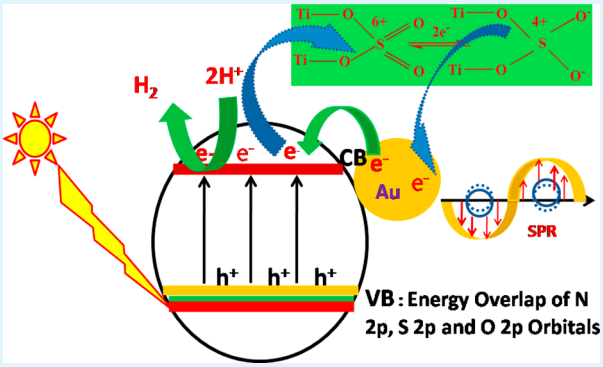

KEYWORDS: *plasmon resonance, Au-SNT, easy channelization, visible light, hydrogen production*

1. INTRODUCTION

The historic invention of Fujishima and Honda in the year 1972 makes TiO_2 as unique and efficient in the area of photocatalysis.[1,2] However, only absorption in UV light due to large band gap energy hinders its application. To stimulate its visible light absorption, much research has been focused on modification of pristine TiO_2. Throughout the last decade, modifications of titania by N^-, S^-, and C^- are regarded to be good photocatalysts.[3−10] However, due to low quantum efficiency in visible range, currently alternative photocatalysts such as plasmonic photocatalysts,[11−15] Z scheme photocatalyst,[16−19]and heretojunction[18,20,21] based materials have been paid much emphasis.

The nanoparticles of Au, Ag, and Pt (noble metals) in the visible light region exhibit a surface plasmon resonance effect (SPR), and this defines the collective movement of conduction band electrons which is stimulated by irradiation of visible light.[14,22] A collective motion of photogenerated electrons from the conduction band towards the surface deposited noble metal nanoparticles is only because of lower fermi energy levels of Au, Ag, and Pt than that of TiO_2.[23−25] These architectural interactions enhance the separation of photogenerated charge carriers as a result retards the rate of recombination which leads in the enhancement of photocatalytic activity. The SPR effect enhances the energy intensity of trapped electrons under the irradiation of visible light as a consequence it enhances the photocatalytic activity.[11,14]

Along with proper excitation and bulk diffusion, surface charge transfer is necessary to reduce the electron hole recombination. Noble metals in the field of photocatalytic water splitting act as co-catalyst which sink photogenerated charge carriers and enhances the activity of photoreaction. Silva et al. synthesized gold supported P25 (titania) and tested its photocatalytic activity for UV and visible light water splitting.[26]

Recently gold nanoisland loaded TiO_2 electrode has been synthesized by Shi et al. and reported that the photocurrent generation and photo catalytic activity depends upon the interfacial structural geometry between the Au nanoisland and TiO_2.[27] Graciani et al.[28] studied the interaction between Au and N and reported that the interaction of preadsorbed Au over N doped TiO_2 appreciably stabilizes the implanted N and consequently enhances the reachable amount of N. Further-

Received: September 10, 2013
Accepted: December 30, 2013
Published: December 30, 2013

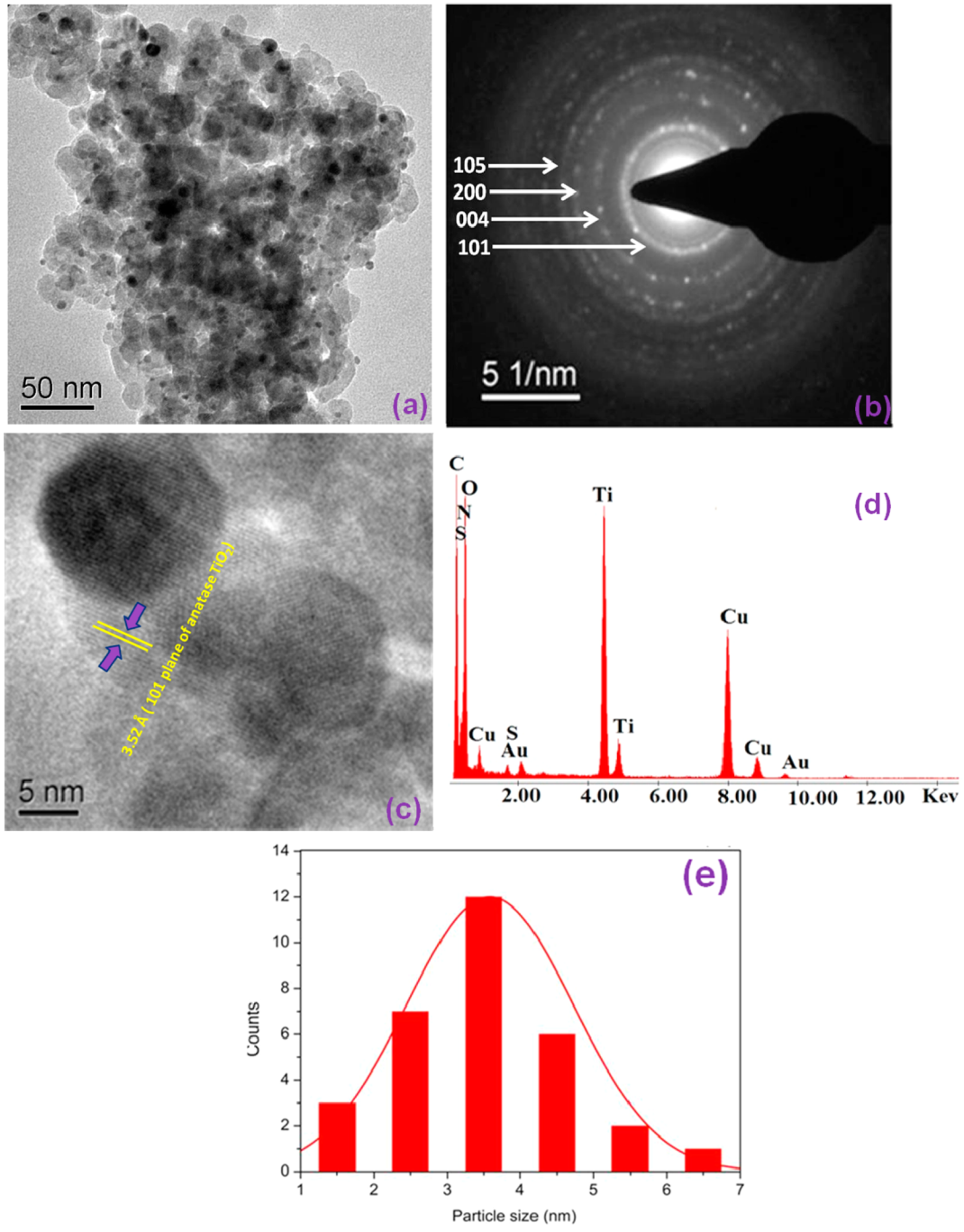

Figure 1. (a) TEM image of 3Au-SNTphotocatalyst. (b) SAED pattern of 3Au-SNT. (c) HRTEM image of 3Au-SNT. (d) EDX spectrum from an arbitrary region showing the presence of N and S in the sample. A large amount of C and some Cu in EDX results arises due to carbon coated Cu grid. (e) Histogram displaying the crystallite size distribution. It is fitted with a Gaussian distribution to determine the average crystallite size and the standard deviation of the size distribution.

more, it has been an active system for the evolution of H_2 gas through water gas shift reaction. However, very few works have been carried out on Au−S interaction on Au−S−TiO_2 systems.[29,30] Our previous work reports the sulfate loading on Au-TiO_2 enhances 5-fold times for catalytic oxidation of CO at room temperature where we have found direct interaction of Au and S in TiO_2 matrix.[30]

Herein, S,N-TiO_2 (SNT) nanocomposites has been synthesized using coprecipitation method and modified by depositing Au through deposition precipitation method in presence of urea. The photocatalytic activity of the two step fabricated (Au-SNT) photocatalyst has been evaluated through water splitting for the generation of H_2 under the irradiation of visible light. The Au modified S,N-TiO_2 has many positive aspects, such as synergetic interaction of nano Au over the surface of S,N-TiO_2, plasmonic resonance, reduction of band gap through N incorporation, sulfate as redox couple, high photocurrent generation, and presence of mesoporosity effectively enhances the charge separation. These properties enhance the photocatalytic activity of Au deposited SNT, and this has been briefly analyzed and discussed.

dx.doi.org/10.1021/am403865r | ACS Appl. Mater. Interfaces 2014, 6, 839−846

2. EXPERIMENTAL SECTION

2.1. Sample Preparation. Titanium oxysulfate sulfuric acid hydrate complex ($TiOSO_4{\cdot}xH_2SO_4{\cdot}xH_2O$), $HAuCl_4$ purchased from Sigma Aldrich, and thiourea from Qualigen were used without doing any further purification. In the present work, we have synthesized SNT nanocomposites by using a soft chemical route which has been reported earlier by us.[6] In the synthesis procedure, the solution was prepared by maintaining the weight ratio of $TiOSO_4$/thiourea/ethanol/water as 13.8:7.6:55.2:77.4. In 69 mL of ethanol, 7.6 g of thiourea was dissolved, and under ice-cold conditions 13.8 g of $TiOSO_4{\cdot}xH_2SO_4{\cdot}xH_2O$ and 77.4 mL of water were added. The prepared solution was stirred up to 3−4 h. For complete precipitation, the resulted transparent solution was heated at 353 K for 5 h. The precipitate was collected by thoroughly washing with distilled water and hot water followed by ethanol to remove all the surface adsorbed impurities and physically adsorbed sulfate species. The obtained precipitate was dried in an oven at 80 °C for 10 h and ground to powder and abbreviated as SNT.

Followed by deposition-precipitation method, Au nano particles have been deposited over SNT by employing urea as the hydrolyzing agent.[31] The as-prepared 1 g SNT was added to 100 mL of aqueous solution of appropriate amounts of $HAuCl_4$ and urea (0.42 M). As $HAuCl_4$ decomposes and is reduced under light, the reaction process was carried out under dark conditions. The suspension was vigorously stirred and thermostatted at 80 °C for 4 h. Then it was centrifuged and washed with water for four times and dried in dark conditions under vacuum at 110 °C for 2 h. The dried solids were calcined for 4 h at a temperature of 400 °C. The samples were abbreviated according to the weight percentage of Au and named as 0.5Au-SNT, 1Au-SNT, 2Au-SNT, 3Au-SNT, 4Au-SNT, and 5Au-SNT.

Characterization. The surface morphologies and the relation to each other on the atomic scale were observed by transmission electronic microscopy (TEM; FEI, TECNAI G^2 20, TWIN) operating at 200 kV. For analysis, the samples were prepared by dispersing the powder in ethanol for 3 min, and then a drop was dripped over carbon coated copper grid and dried. By using the Gatan CCD camera, the TEM images were captured and the particle size was measured by using the IMAGEJ analysis package. To identify the phase and structure, powder X-ray diffraction (XRD) was carried out on a Rigaku Miniflex powder diffraction meter (setting the voltage and current at 30 KV and 15 mA) using Cu Kα radiation (λ = 1.54 Å). The diffraction patterns were recorded within the range of $5° < 2\theta < 70°$ with a scan rate of 2°/min.

At liquid nitrogen temperature (−196 °C), N_2 adsorption-desorption studies were carried out on ASAP 2020 (Micromeritics) instrument. Prior to analysis under vacuum conditions (10^{-5} Torr), the samples were degassed at 200 °C for 4 h. Surface area has been analyzed by Brunauer−Emmett−Teller (BET) method through the adsorption data within the p/p_0 range from 0.05 to 0.33. The pore volumes were occupied at relative pressure (p/p_0) of 0.95 and the pore size distribution has been calculated by using the Barrett−Joyner−Halenda (BJH) equation from the desorption branch of the isotherm.

The optical absorbance properties of all these photocatalyst were tested via UV−vis spectrometer (Varian Cary 100) in the visible region (200−800 nm) by using boric acid as the reference. To investigate the electronic states, X-ray photoelectron spectroscopy (XPS) was performed on a Kratos Axis 165 instrument with a dual anode Mg and Al apparatus using the Mg Kα source. The binding energy was calibrated by using the C1s peak of carbon at 284.6 as reference. The XPS peaks are deconvoluted through using Origin Pro 7.0 software by fitting curves with Gaussian distribution function. The atomic concentration (C_x) has been calculated by using the following eq 1.

$$C_x = (I_x/S_x)/\sum_{\alpha} I_\alpha/S_\alpha \quad (1)$$

where I_x is the relative peak area, S_x is the sensitivity factors for respective element, and α represents other component elements to the system.

For photoelectrochemical measurement, SNT and 3Au-SNT film electrodes were prepared through electrophoretic deposition method over the conducting glass supports (F-doped SnO_2). The current voltage was measured by using a conventional pyrex electrochemical cell, and it contained the prepared electrode as working electrode and a platinum wire and Ag/AgCl electrode as the counter and reference electrode, respectively. Through a potentiostat, the potential of the working electrode was controlled. The cell was filled with 0.1 M Na_2SO_4, and its pH was adjusted to 5.9. Before the electrochemical analysis, the electrolyte was saturated with argon gas, and through a potentiostat (HZ-5000, Hokuto Denko; SDPS-501c, Syrinx) the potential of the electrode was controlled. Irradiation was carried out through the conducting glass using a xenon lamp of 300 W with a cold mirror and cutoff filters (Hoya) as necessary.

2.2. Photocatalytic Hydrogen Production. The catalytic activity has been evaluated by water splitting for the evolution of hydrogen gas according to the technique reported earlier by us.[8] In a batch reactor, the catalytic activity and deactivation have been studied. The experiment was carried out by taking 0.05 g of catalyst in 50 mL of 10 vol % methanol solution, and the solution was stirred with a magnetic stirrer to prevent the particles from settling down at the bottom of the reactor. Before irradiation from the visible light source, the solution in the reactor was purged with N_2 gas for several times to remove the dissolved gases. In this process, a 125 W medium pressure Hg lamp was used as light source and 1 M $NaNO_2$ solution as UV filter. The gas evolved during the reaction process was collected by using the water displacement technique and analyzed it in the GC-17A (Shimadzu) using 5 Å molecular sieve column and a thermal conductivity detector (TCD). A comparison of the retention time of the peak that appeared on the chromatogram with the standard confirmed that the evolved gas was hydrogen. According to Lianos et al., the approximate average incident radiation power on the photocatalyst and stored chemical energy for 3Au-SNT photocatalyst under the irradiation of visible light has been calculated and it has been found to be 120 mW and 21.23 mW, respectively.[32] Therefore, using eq 2, energy conversion efficiency of the photocatalyst has been calculated.

$$\text{conversion efficiency (\%)} = \text{stored chemical energy/incident light energy} \times 100 \quad (2)$$

3. RESULTS AND DISCUSSION

3.1. Structural Features. Figure 1 represents the TEM image of best performing 3 wt % Au-SNT photocatalyst. From Figure 1a, it is clearly evident that the Au nanoparticles are uniformly dispersed throughout the well connected TiO_2 nanoparticles and the observed disordered mesoporous morphology is because of the intergrowth of fundamental particles. These aggregations of fundamental particles form extra framework void space. The observed morphology has been well consistent with the observed N_2 sorption isotherms and will be analyzed in the next part. Figure 1b depicts the selected area electron diffraction (SAED) pattern of nanocrystalline particles. The pattern clearly reveals bright concentric rings, and it is due to the diffraction from (101), (004), (200), and (105) planes of anatase TiO_2. In the pattern, the intense diffraction plane, that is, (101), highlighting the TiO_2 crystallite is preferentially oriented along (101) plane.

From the HRTEM image (Figure 1c), the lattice fringes with an interplanar spacing of 3.52 Å are observed and assigned to the 101 plane of anatase TiO_2. The HRTEM image confirmed the crystalline character of the 3Au-SNT photocatalysts. Energy dispersive X-ray (EDX) analysis was carried out at random spots over the 3Au-SNT specimen to confirm the chemical composition, and is shown in Figure 1d. The spectrum reveals

existence of Au, N, S, O, and Ti, and it confirms well distribution of Au, N, and S in TiO_2 lattice.

Figure 1e represents the particle size distribution of Au in 3Au-SNT. It has been well fitted to the Gaussian function and found a narrow nanocrystallite size distribution with an average particle size of 3.5 ± 0.2 nm with a standard deviation of σ = 0.78 ± 0.2 nm. By using various TEM micrographs and IMAGEJ analysis package these values are calculated. The low particle size of Au (3.5 nm) deposited on nearly 12 nm size of anatase TiO_2 (calculated from TEM) could be effective for photocatalytic purpose.[33]It has been seen that low particle size Au nanoparticles (usually smaller than 5 nm) display excellent photocatalysis[23] as well as CO oxidation.[29]

The phase identity of the as-prepared photocatalyst has been confirmed through powder XRD analysis and is depicted in Figure 2. The patterns reveals that different weight percent of

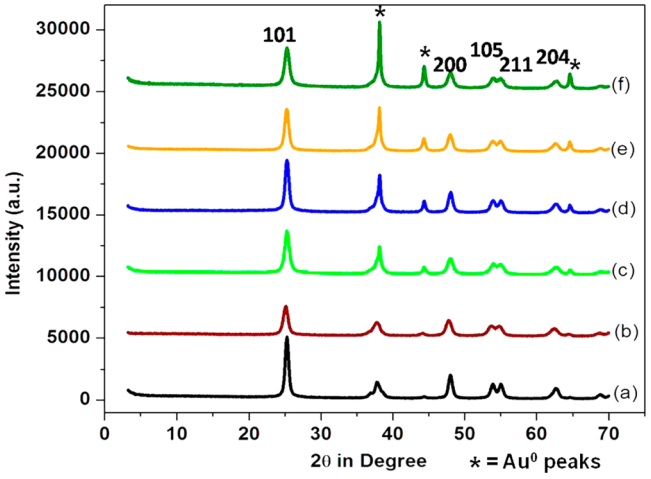

Figure 2. XRD patterns of (a) 0.5Au-SNT, (b) 1Au-SNT, (c) 2Au-SNT, (d) 3Au-SNT, (e) 4Au-SNT, and (f) 5Au-SNT samples.

Au loaded SNT exhibits both anatase phase of TiO_2 and metallic Au crystallites. The characteristic peaks at 38.2, 44.4 and at 64.6° confirm the deposited Au mainly exist in the form of Au^0 on the surface of SNT.[34] The increase in gold content from 0.5 to 5 wt % enhances the peak intensity and was attributed to 111, 200, and 220 reflections of metallic gold.[35] All other reflections correspond to anatase TiO_2. From the XRD pattern, it has been confirmed the high crystallization of the anatase phase.

3.2. BET Surface Area Analysis. The N_2 adsorption-desorption isotherm of Au-SNT nanocomposites has been shown in Figure 3. The physicochemical properties of all the as prepared photocatalyst are depicted in Table 1. The figure clearly reveals that all these samples exhibit type IV isotherm and its hysteresis loop indicates H1 type (according to IUPAC nomenclature) suggesting the existence of well developed of mesoporosity. Earlier in our study, we observed interparticle mesoporosity for SNT nanocomposites, and this might be due to aggregation of smaller particles.[6]

Here, the observed results demonstrate that SNT photocatalyst exhibits specific surface area of 132 m^2/g. However, Au deposited SNT photocatalysts showed drastic decrease in specific surface which lies in the range of 90−116 m^2/g. The comparison study reveals that sulfate incorporation to the TiO_2 network in SNT photocatalyst may hinder the crystallite growth as well as maintain the mesoporous network.[9,36,37]

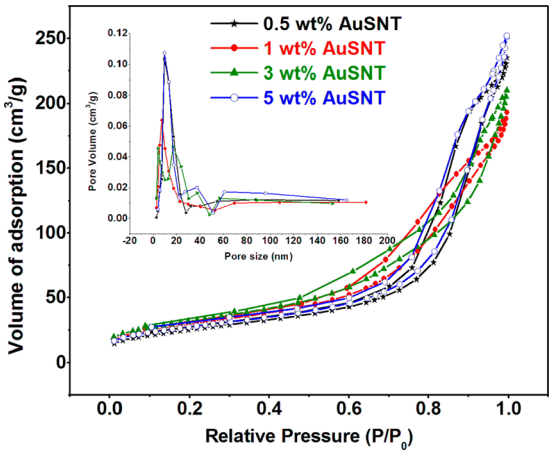

Figure 3. N_2 adsorption and desorption study of Au-SNT catalyst.

Table 1. Crystallite Size and Textural Properties of SNT and Au-SNT Samples

photocatalyst	Au particle size (nm)[a]	BET surface area (m^2/g)[b]	pore size (nm)[b]	pore volume (cm^3/g)[b]
SNT		132	4.6	0.13
1Au-SNT	4.2	116.3	8.7	0.30
3Au-SNT	3.5	115.3	9.0	0.33
5Au-SNT	5.2	98.4	12.3	0.39

[a]Calulated from TEM study. [b]Measured from N_2 sorption studies

However, the reduction of specific surface area in Au promoted TiO_2 might be due to the decrease of sulfur concentration which has been well supported by XPS study. Besides this, deposition of Au to SNT may partly fill up the pores and retard the specific surface area. Here, in this work, the observed decrease in specific surface area is well consistent with the obtained pore size value; that is, increased value of pore size suggests decrease in specific surface area.[38]

The inset in Figure 3 depicts the pore size distribution curve. It reveals Au-SNT has pronounced mesoporosity and narrow pore size distribution with an average pore diameter between 8 and 13 nm. The well developed mesoporous architecture, pore order, and high surface area makes the system pivotal in the field of photocatalysis, that is, due to the enhanced ability of light harvestation and molecular transportation of reactant and products.

3.3. Spectroscopic Investigations. Figure 4 represents the UV−vis spectra for Au-SNT photocatalyst. It has been well known that absorption edge of anatase TiO_2 lies in the region 380 nm. UV−vis absorbance spectra of Au-SNT photocatalyst (Figure 4) reveal enhanced absorption in the visible region. The enhanced absorption is because of collective oscillation of electron in the nano Au particle stimulated by optical excitation.[39] The peak corresponding to 590 nm (500−700 nm broad peak) attributed surface Plasmon energy state and confirms the production of energies electron.[29] The intensity of plasmon absorbance band depends on the gold content, particle size of gold and the surrounding environment.[29,31] In case of 3Au-SNT, the absorption of gold was found to be greater than 600 nm in comparison to Au-TiO_2 (550 nm). The resulting red shifting of the plasmon band in Au-SNT might be ascribed to the interaction of nano Au and SNT support.[40] However, the higher content of gold (5 Au-SNT) in the system not only affects the penetration ability of light but also behaves as the

dx.doi.org/10.1021/am403865r | ACS Appl. Mater. Interfaces 2014, 6, 839−846

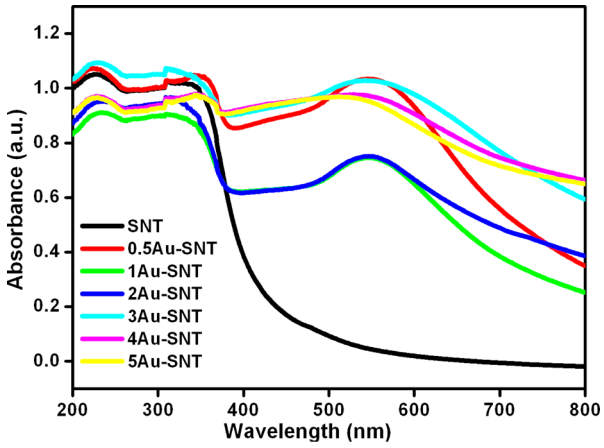

Figure 4. UV−vis DRS of SNT and various wt % Au loaded SNT samples.

recombination center, and as a result it lowers the photocatalytic activity.[31]

Figure 5 represents the XPS spectrum for Au SNT nanocomposites, with (a) N1s, (b) S2p, (c) Au(4f), (d) Ti(2p), and (e) O(1s) core levels. The observed N1s spectrum deconvoluted into three peaks at ca. 399.7, 400.1, and 401.1 eV.

The peak at the region of 399.7 eV attributed to O−Ti−N linkage, which signifies a marked contribution of anionic N^- in TiO_2 lattice.[9,41] It has been well reported that substitutional N doping is more effective toward visible light absorption though it reduces the energy gap and forms a localized state above the valence band.[4] Two more peaks appeared at around 400.1 and at 401.1 eV, suggesting the presence of oxidized N (i.e O−N−Ti) or some surface oxidation state and it also have some important roles in the catalytic performances.[8,9] The above observed results confirmed the presence of two types of nitrogen environment within the material.

Figure 5b depicts XPS spectra for S 2p and the binding energy peak appeared at around 168.5 eV.[9,29] The peak at 168.5 attributed to incorporation of SO_4^{2-} to the TiO_2 lattice. Though this group (SO_4^{2-}) cannot be incorporated into the TiO_2 lattice, it may chemisorbed and exist in the form of bidentate linkage with Ti^{4+}.[6,9] The bidendate sulfate exists as S^{6+}cation.

Figure 5c depicts XPS spectra for Au(4f). The two peaks appeared at the binding energy of 83.0 eV (Au $4f_{7/2}$) and 86.7 eV (Au $4f_{5/2}$) are assigned to metallic gold Au^0.[42] No noticeable peak at higher binding energy confirms absence of oxidized gold species.

Figure 5d depicts the XPS spectra for Ti(2p). For pure TiO_2 the Ti $2p_{3/2}$ peak appeared at 459 eV.[8] In the present investigation, it appeared at around 458.2 eV (Ti $2p_{3/2}$) and at 464.1 eV (Ti $2p_{1/2}$). The comparison study with pure TiO_2 reveals slight shifting of Ti $2p_{3/2}$ which suggests the parent Ti^{4+} is partially reduced and it might be because of strong interaction of SO_4^{2-} and lattice incorporation of N which changed the electron density distribution around Ti. The XPS peak for O1s is shown in Figure 5e. The peak appeared at around 529.9 eV correspond to oxygen in TiO_2. The amounts of N, S, and Au content was calculated from XPS peaks and are shown in Table 2.

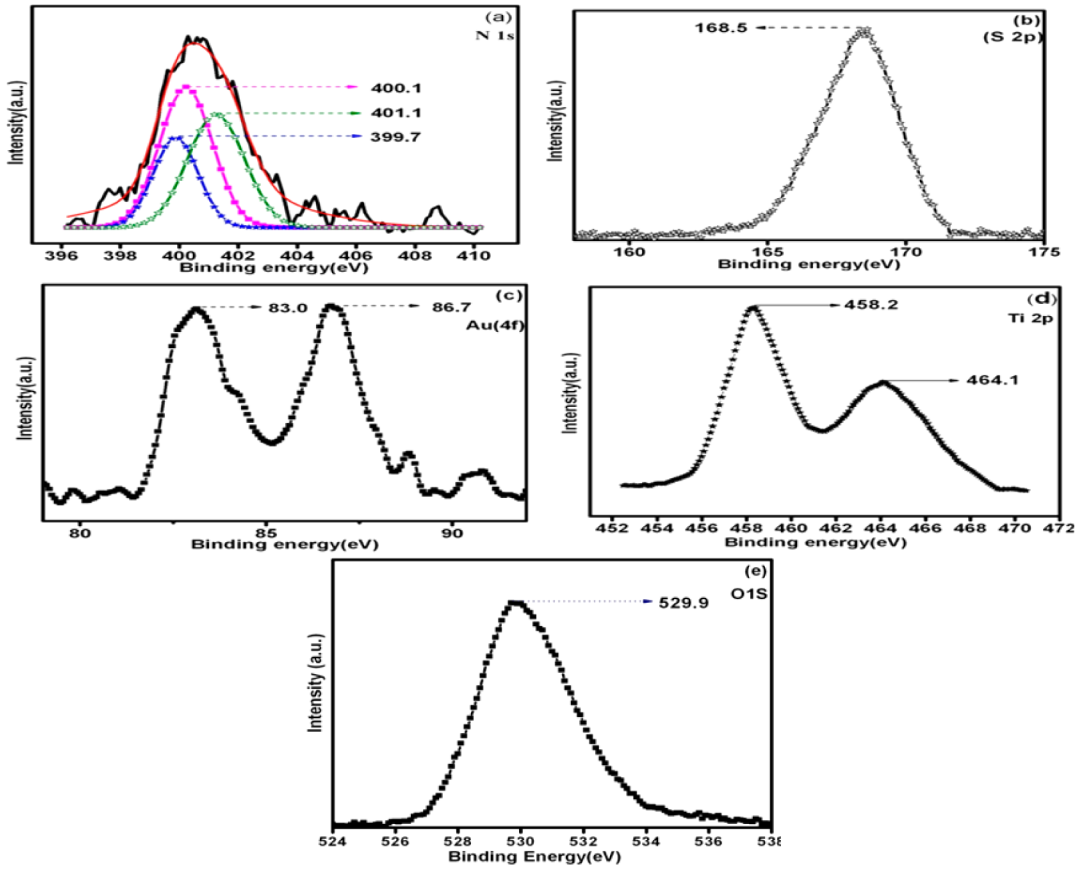

Figure 5. XPS core level peaks of 3Au-SNTsamples.

dx.doi.org/10.1021/am403865r | ACS Appl. Mater. Interfaces 2014, 6, 839−846

Table 2. N and S, Au content, optical properties and H_2 generation of SNT and Au-SNT samples

photocatalyst	N content (atom %)	S content (atom %)	Au content (atom %)	band gap energy (eV)	H_2 gas evolved (μmol/h)	conversion efficiency (%)
NT	0.76			2.9	20	1.31
ST		2.3		3.0	22.6	1.49
SNT	0.91	2.5		2.8	31.2	2.04
1Au-SNT	0.95	1.0	0.9	2.3	148.8	9.8
3Au-SNT	1.07	0.8	2.7	2.2	267.6	17.6
5Au-SNT	1.1	0.6	4.2	2.3	90.0	5. 9

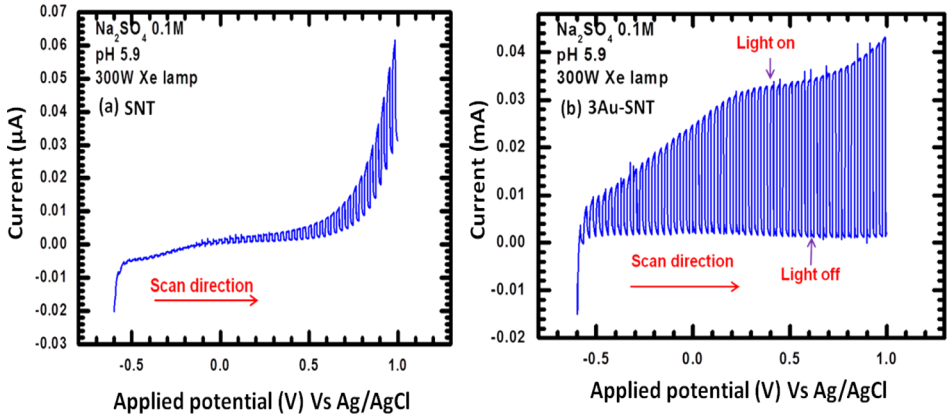

Figure 6. Current–potential relationship for SNT and 3Au-SNT photoelectrodes.

3.4. Photocurrent Measurement. Photoelectrochemical measurement was carried out to observe the photoelectric behavior of SNT and 3Au-SNT. It has been carried out by using SNT and 3Au-SNT film prepared as photoelectrode. In a three-electrode setup flask with 0.1 M Na_2SO_4 solution (maintaining pH at 5.9), the photocurrent was measured. The current–potential relationship for SNT and 3Au-SNT photoelectrodes is shown in Figure 6. The current–potential diagram demonstrates an anodic photocurrent generation with respect to the applied potential and an increased magnitude in positive direction suggests that the as prepared SNT and 3Au-SNT photoelectrodes have n-type semiconducting character. From the photocurrent spectra, a low anodic current noticed for SNT than that of the 3Au-SNT photoelectrode. Loading of Au to SNT nanocomposite is mostly responsible for enhancement of the photocurrent with applied bias. The high photocurrent generation might be due to the interfacial structure between Au and SNT as well as SPR effect assist for transformation of electron from Au to SNT.[27]

Figure 7 shows the photoresponse spectra of 3Au-SNT with various cut-off wavelengths of incident light. The photocurrent values were produced by irradiating the photocatalyst with suitable cutoff filters for the wavelength, and it has been observed a decrease in photon counts with increasing wavelength. When 3Au-SNT was irradiated with light, it generated photocurrent. It generates a maximum amount of photocurrent when irradiated with incident light of wavelength greater than 350 nm ($\lambda \geq 350$ nm). From the figure, it demonstrates gradual decrease in photocurrent with respect to increase in wavelength, that is, up to 420 nm. However, when the photoelctrode was irradiated with incident light of greater than 420 nm, the generation of photocurrent again increases with increase in the wavelength. The photocurrent reaches its maximum value at 590 nm. This dramatic enhancement of photocurrent is well consistent to the observed DRUV–vis

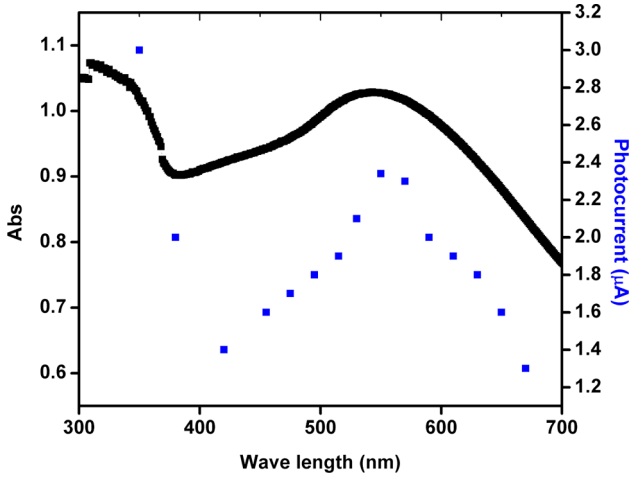

Figure 7. Photoresponse spectra of 3Au-SNT with various cutoff wavelengths of incident light.

spectra shown in Figure 7 and it is due to the SPR effect of the Au.

3.5. Photocatalytic Activity. To evaluate the photocatalytic activity, photocatalysts were tested for water splitting under visible light irradiation ($\lambda \geq 400$ nm) for the evolution H_2 gas. No noticeable H_2 evolution has been found in the absence of light or photocatalyst. The H_2 evolution for SNT and Au-SNT photocatalyst is shown in Figure 8. All these photocatalysts are active toward H_2 evolution under the irradiation of visible light.

Among all these photocatalysts, the highest activity for H_2 evolution has been noticed for 3Au-SNT at ca. 267.6 μmol/h (shown in Table 2). In the initial 5 h of the reaction conditions, it would able to evolve 1382.6 μmol of H_2 gas. Recyclability test was performed to confirm the stability of the highest result performed by photocatalyst (3Au-SNT), and results are shown in Figure 9. To check the stability, the reactor was evacuated

dx.doi.org/10.1021/am403865r | ACS Appl. Mater. Interfaces 2014, 6, 839–846

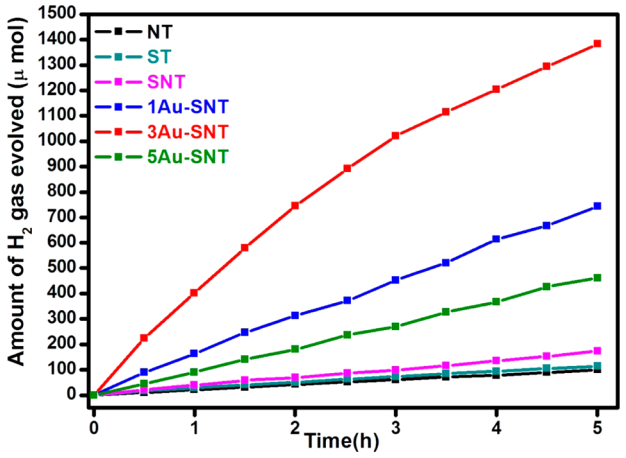

Figure 8. Time course of H_2 evolution over SNT and various wt % Au loaded SNT samples.

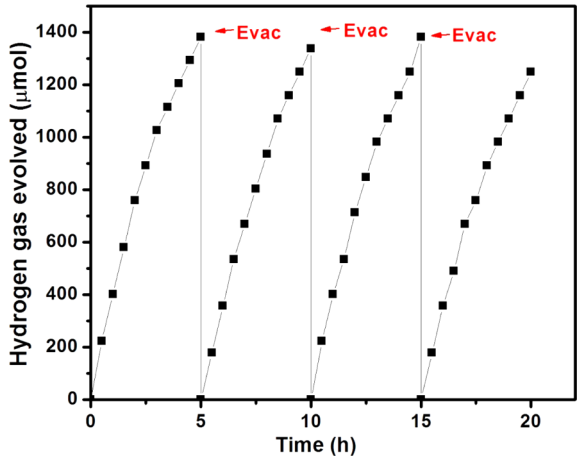

Figure 9. Reusability study over 3Au-SNT for H_2 evolution under visible light irradiation.

and purged with N_2 gas in every 5 h of the reaction and the experiment was carried out for four cycles. In each reaction, almost same activity has been found, and it confirms the stability. Our previously synthesized N-TiO_2 and S-TiO_2[6] under visible light irradiation could able to evolve only 20 and 22.6 μmol/h (Table 2), respectively. However. Au-TiO_2 and SNT could generate 15.1 and 31.2 μmol/h of hydrogen gas, respectively. As compared to SNT, the photocatalytic activity is significantly enhanced by loading Au nanoparticles. Under the irradiation of visible light, 3Au-SNT generates the highest amount of hydrogen gas (267.6 μmol/h) than other Au loaded SNT photocatalysts. The observed activity for 3Au-SNT has been found to be 9 times higher in comparison to that of pristine SNT. This shows that Au and SNT have significant characteristics in the photocatalytic application of Au-SNT. As the Fermi level energy of Au is lower to SNT, the photoexcited electrons from the conduction band of SNT move easily to the Au nanoparticles.[25] These processes help effective separation of photogenerated charge carriers, and as a consequence it reduces the recombination process. A greater number of electrons accumulates over the surface of nano Au particle due to SPR effect. The accumulation of electron on Au nanoparticles shifts the position of the Fermi energy level closer to the conduction band of SNT.[25] So the electrons flow from the more negative shifted energy level of Au nanoparticle to the conduction band of SNT and efficiently reduce the protons to form hydrogen gas. In this way, Au nanoparticle efficiently enhances the H_2 generation under the irradiation of visible light.[25,39,43]

The greatest advantage of the present investigation is that gold plays a versatile role in the photocatalytic performance: it acts as co-catalyst so there is no need to use any other noble metals, and it also supports the light harvestation of SNT. On the other hand, low photocatalytic activity has been observed for higher content of gold promoted SNT (5Au-SNT). This may be due to the fact that high content of gold may block the surface active sites as well as hinder the light to reach the target surface, hence lowering the photocatalytic activity.[44]

In addition to the ideal property of Au nanoparticles, the presence of N in the crystal lattice of TiO_2 successfully reduces the band gap and helps to shift the optical absorbance toward the visible region. The incorporation of N in TiO_2 exists in the form of N−Ti−O which partially converts the system from Ti^{4+} to Ti^{3+} and effectively contributes toward visible light absorption.[6,9] Existence of sulfate has also an important role toward enhanced photocatalytic activity. It facilitates the electron transfer and consequently increases the forward reduction reaction. The electrons from the conduction band move toward the most electropositive S atom of the sulfate species and reduce it from S^{6+} to S^{4+}, and then the electrons are transferred to the Au co-catalyst to retain the system as S^{6+}.[6,9,45] Here the bidentate species are reduced as well as regenerated, which signifies its stable photoactivity.[6,46]The synergetic effect of Au and sulfate as redox couple has potential role for enhanced photocatalytic activity.

Both Au and sulfate act as co-catalyst and effectively minimize the recombination of charge carriers. Besides this, the retention of mesoporous frame enhances light harvestation properties as well as easy diffusion of charge carriers toward the active sites making, the system pivotal for excellent visible light photocatalysis. The beauty of the present photocatalyst is that it is the first ever such catalyst which synergetically combines all the photocatalytic fundamental necessities within its electronic environment. The mechanism of photocatalytic hydrogen production over Au-SNT photocatalysts is shown in Scheme 1. So overall, synergetic combination of surface plasmon resonance, low particle size of nano Au (3.5 nm), low band gap energy, high photocurrent generation, and effective charge transfer are the origin of high photocatalytic water splitting in 3 wt % Au promoted SNT samples. The energy conversion

Scheme 1. Mechanism of Light Harvestation, Plasmonic Property of Au and Sulfate as Redox Couple toward Hydrogen Production under Visible Light

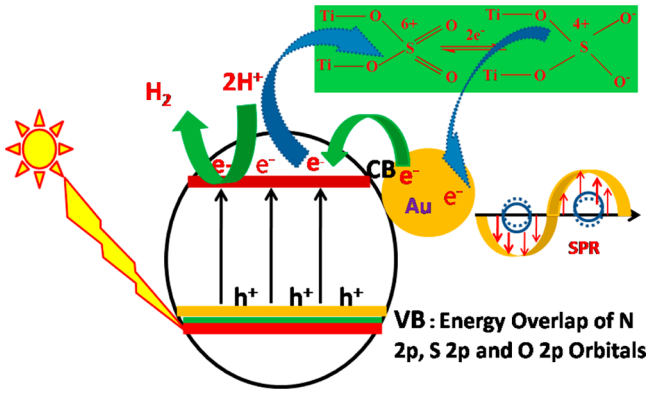

dx.doi.org/10.1021/am403865r | ACS Appl. Mater. Interfaces 2014, 6, 839−846

efficiency for the best performed photocatalyst, that is, Au-SNT, was found to be 17.6% for the production of H_2 under the irradiation of visible light.

4. CONCLUSIONS

Au nanoparticles have been successfully deposited on SNT by deposition precipitation method which enhance the light harvestation property in the visible range due to surface plasmon resonance property and also increase the surface charge separation process. There is no need for any external co-catalyst and redox couple. The presence of mesoporosity and interconnective morphology between the nanoparticles and sulfate modification enhances the charge separation and suppresses the recombination. The hydrogen generation activity of 3Au-SNT is nearly 9 times higher than that of neat SNT with an energy conversion efficiency of 17.6%. The synergetic effects of surface plasmon resonance, low particle size of nano Au (3.5 nm), low band gap energy, high photocurrent generation, and effective charge transfer enhances stability and the photocatalytic hydrogen production under visible light.

AUTHOR INFORMATION

Corresponding Author

*E-mail: paridakulamani@yahoo.com, kmparida@immt.res.in. Tel.: +91-674-2379425. Fax: +91-674-258163.

Notes

The authors declare no competing financial interest.

ACKNOWLEDGMENTS

We are thankful to Prof. B. K. Mishra, Director, CSIR-Institute of Minerals and Materials Technology, Bhubaneswar for the support and permission to publish the paper. The financial support from CSIR in form of NWP-56 is greatly acknowledged. S.P. is thankful to CSIR, New Delhi for the award of SRF.

REFERENCES

(1) Chen, X.; Shen, S.; Guo, L.; Mao, S. S. *Chem. Rev.* **2010**, *110*, 6503−6570.
(2) Fujishima, A.; Honda, K. *Nature* **1972**, *238*, 37−38.
(3) Asahi, R.; Morikawa, T.; Ohwaki, T.; Aoki, K.; Taga, Y. *Science* **2001**, *293*, 269−271.
(4) Sathish, M.; Viswanathan, B.; Viswanath, R. P.; Gopinath, C. S. *Chem. Mater.* **2005**, *17*, 6349−6353.
(5) Parida, K. M.; Naik, B. *J. Colloid Interface Sci.* **2009**, *333*, 269−276.
(6) Naik, B.; Parida, K. M.; Gopinath, C. S. *J. Phys. Chem. C* **2010**, *114*, 19473−19482.
(7) Naik, B.; Parida, K. M.; Behera, G. C. *ChemCatChem* **2011**, *3*, 311−318.
(8) Parida, K.M.; Pany, S.; Naik, B. *Int. J. Hydrogen Energy* **2013**, *38*, 3545−3553.
(9) Pany, S.; Parida, K. M.; Naik, B. *RSC Adv.* **2013**, *3*, 4976−4984.
(10) Martha, S.; Das, D. P.; Biswal, N.; Parida, K. M. *J. Mater. Chem.* **2012**, *22*, 10695−10703.
(11) Awazu, K.; Fujimaki, M.; Rockstuhl, C.; Tominaga, J.; Murakami, H.; Ohki, Y.; Yoshida, N.; Watanabe, T. *J. Am. Chem. Soc.* **2008**, *130*, 1676−1680.
(12) Tian, Y.; Tatsuma, T. *J. Am. Chem. Soc.* **2005**, *127*, 7632−7637.
(13) Ingram, D. B.; Linic, S. *J. Am. Chem. Soc.* **2011**, *133*, 5202−5205.
(14) Chen, J. J.; Wu, J. C. S.; Wu, P. C.; Tsai, D. P. *J. Phys. Chem. C* **2011**, *115*, 210−216.
(15) Jones, M. R.; Osberg, K. D.; Macfarlane, R. J.; Langille, M. R.; Mirkin, C. A. *Chem. Rev.* **2011**, *111*, 3736−3827.
(16) Sasaki, Y.; Nemoto, H.; Saito, K.; Kudo, A. *J. Phys. Chem. C* **2009**, *113*, 17536−17542.
(17) Fu, N.; Jin, Z.; Wu, Y.; Lu, G.; Li, D. *J. Phys. Chem. C* **2011**, *115*, 8586−8593.
(18) Maeda, K.; Higashi, M.; Lu, D.; Abe, R.; Domen, K. *J. Am. Chem. Soc.* **2010**, *132*, 5858−5868.
(19) Xu, Q. C.; Wellia, D. V.; Ng, Y. H.; Amal, R.; Tan, T. T. Y. *J. Phys. Chem. C* **2011**, *115*, 7419−7428.
(20) Etacheri, V.; Seery, M. K.; Hinder, S. J.; Pillai, S. C. *Chem. Mater.* **2010**, *22*, 3843−3853.
(21) Chen, C.; Cai, W.; Long, M.; Zhou, B.; Wu, Y.; Wu, D.; Feng, Y. *ACS Nano* **2010**, *4*, 6425−6432.
(22) Merlen, A.; Gadenne, V.; Romann, J.; Chevallier, V.; Patrone, L.; Valmalette, J. C. *Nanotechnology* **2009**, *20*, 1−7.
(23) Li, H.; Bian, Z.; Zhu, J.; Huo, Y.; Li, H.; Lu, Y. *J. Am. Chem. Soc.* **2007**, *129*, 4538−4539.
(24) Li, X.; Fan, T.; Zhou, H.; Zhu, B.; Ding, J.; Zhang, D. *Microporous Mesoporous Mater.* **2008**, *116*, 478−484.
(25) Ni, M.; Leung, M. K. H.; Leung, D. Y. C.; Sumathy, K. *Renewable Sustainable Energy Rev.* **2007**, *11*, 401−425.
(26) Silva, C. G.; Juarez, R.; Marino, T.; Molinari, R.; Garcia, H. *J. Am. Chem. Soc.* **2011**, *133*, 595−602.
(27) Shi, X.; Ueno, K.; Takabayashi, N.; Misawa, H. *J. Phys. Chem. C* **2013**, *117*, 2494−2499.
(28) Graciani, J. S.; Nambu, A.; Evans, J.; Rodriguez, J. A.; Sanz, J. F. *J. Am. Chem. Soc.* **2008**, *130*, 12056−12063.
(29) Parida, K. M.; Sahu, N.; Tripathi, A. K.; Kamble, V. S. *Environ. Sci. Technol.* **2010**, *44*, 4155−4160.
(30) Mohapatra, P.; Moma, J.; Parida, K. M.; Jordaan, W. A.; Scurrell, M. S. *Chem. Commun.* **2007**, 1044−1046.
(31) Wu, Y.; Liu, H.; Zhang, J.; Chen, F. *J. Phys. Chem. C* **2009**, *113*, 14689−14695.
(32) Strataki, N.; Bekiari, V.; Kondarides, D. I.; Lianos, P. *App. Catal., B* **2007**, *77*, 184−189.
(33) Baiju, K. V.; Shukla, S.; Sandhya, K. S.; James, J.; Warrier, K. G. K. *J. Phys. Chem. C* **2007**, *111*, 7612−7622.
(34) Zhang, J.; Xiao, L.; Cong, Y.; Anpo, M. *Top. Catal.* **2008**, *47*, 122−130.
(35) Debeila, M. A.; Coville, N. J.; Scurrell, M. S.; Hearne, G. R.; Witcomb, M. J. *J. Phys. Chem. B* **2004**, *108*, 18254−18260.
(36) Mohapatra, P.; Parida, K. M. *J. Mol. Catal. A: Chem.* **2006**, *258*, 118−123.
(37) Samantray, S. K.; Parida, K. M. *J. Mater. Sci.* **2004**, *39*, 1−14.
(38) Biswal, N.; Das, D.P.; Martha, S.; Parida, K. M. *Int. J. Hydrogen Energy* **2011**, *36*, 13452−13460.
(39) Subramanian, V.; Wolf, E. E.; Kamat, P. *J. Am. Chem. Soc.* **2004**, *126*, 4943−4950.
(40) Parida, K. M.; Sahu, N.; Mohapatra, P.; Scurrell, M. S. *J. Mol. Catal. A: Chem.* **2010**, *319*, 92−97.
(41) Li, X.; Zhang, H.; Zheng, X.; Yin, Z.; Wei, L. *J. Environ. Sci.* **2011**, *23*, 1919−1924.
(42) Hidalgo, M. C.; Maicu, M.; Navıo, J. A.; Colon, G. *J. Phys. Chem. C* **2009**, *113*, 12840−12847.
(43) Jakob, M.; Levanon, H.; Kamat, P.V. *Nano Lett.* **2003**, *3*, 353−358.
(44) Martha, S.; Reddy, K. H.; Biswal, N.; Parida, K.M. *Dalton Trans.* **2012**, *41*, 14107−14116.
(45) Sun, H.; Liu, H.; Ma, J.; Wang, X.; Wang, B.; Han, L. *J. Hazard. Mater.* **2008**, *156*, 552−559.
(46) Liang, C.; Bruell, C. J.; Marley, M. C.; Sperry, K. L. *Chemosphere* **2004**, *55*, 1213−1223.